www.springer.com/41230
https://doi.org/10.1007/s41230-025-4070-9
Research & Development
Vol. 22 No. 3 May 2025
CHINA FOUNDRY

Mechanical properties and microstructures of Mg-6Si alloys fabricated using the tungsten-inert-gas arc additive manufacturing

Peng-cheng Zhou[1], *Guo-qiang You[1, 2, 3], Jin-yu Feng[1], Lei Wang[1], Xiao Lin[1], and Bin Jiang[1, 2, 3]

1. College of Materials Science and Engineering, Chongqing University, Chongqing 400044, China

2. National Engineering Research Center for Magnesium Alloys, Chongqing University, Chongqing 400044, China

3. National Key Laboratory of Advanced Casting Technologies, Chongqing University, Chongqing 400044, China

Abstract: Si-containing Mg alloys solidified at conventional rates often contain coarse and sharp Mg_2Si phases, which can result in inferior material properties. In this study, Mg-6wt.% Si (Mg-6Si) alloy was prepared by wire arc additive manufacturing (WAAM), employing the gas tungsten arc welding technique with rapid cooling. The microstructures and mechanical properties of the WAAM alloy were investigated and compared with those of the as-cast samples produced using a metal mold. The results indicate that the WAAM Mg-6Si is harder and stronger than the as-cast samples. The microhardness of the WAAM Mg-6Si increases by 36.6% in comparison to that of as-cast Mg-6Si alloy. Furthermore, the average tensile strengths at room temperature and 150 °C increases by 63.4% and 21.3%, respectively. WAAM refines both the Mg_2Si phase and the overall grains, resulting in a homogeneous morphology and improved mechanical properties. The granular Mg_2Si phase, characterized by fine particles with a diffused distribution, shows a significant increase in concentration. The acicular Mg_2Si phase is distributed along the grain boundaries, and its concentration significantly decreases. The average grain size of the Mg_2Si phase is about 9.20 μm, about 5 times smaller. The refinement and distribution of the granular Mg_2Si phase, as well as the reduction in the amount of needle-like Mg_2Si particles, are the key factors for improving the mechanical properties of WAAM Mg-6Si alloy.

Keywords: arc additive manufacturing; magnesium alloy; Mg_2Si; microstructure; gas tungsten arc welding

CLC numbers: TG146.22 **Document code:** A **Article ID:** 1672-6421(2025)03-263-10

1 Introduction

Mg alloys are promising lightweight materials owing to their low density (approximately 1.74 g·cm^{-3}), high specific strength, excellent damping and vibration reduction properties, and outstanding electrical and thermal conductivities. They have a wide range of applications in various sectors including aerospace, automotive, rail transportation, and consumer electronics (3C products) [1, 2]. Numerous Mg alloys have been developed, including those containing Si in the Mg_2Si reinforced phase. This phase is known for its high hardness (4.5 GPa), high elastic modulus (120 GPa), low density (1.93 g·cm^{-3}), high melting point (1,085 °C), and low coefficient of thermal expansion (7.5×10^{-6} K^{-1}) [3, 4]. However, the morphology of the primary phase of Mg_2Si under solidification conditions is highly sensitive to the solidification rate. It tends to coarsen when solidified by conventional casting, which degrades mechanical properties and limits engineering applications of the Mg alloys [5]. For achieving a desirable morphology of the Mg_2Si phase, there are two main approaches: (1) adding elements such as P, Sb, Sr, Zn, Ca, and Re to modify the Mg_2Si phase [6-11], and (2) achieving higher solidification rates via process control to refine the Mg_2Si phase [12-14].

Additive manufacturing technology is becoming increasingly mature and has industrial applications in the small-batch manufacturing of complex-shaped parts. Wire arc additive manufacturing (WAAM), as a rising additive manufacturing method, has unique safety advantages for Mg alloys owing to the use of wires rather than powder as the raw material [15, 16].

*Guo-qiang You
Male, Ph. D. His research interests mainly focus on high-performance magnesium alloy and advanced welding technology.
E-mail: ygq@cqu.edu.cn
Received: 2024-04-07; Revised: 2024-06-23; Accepted: 2024-08-14

In wire arc additive manufacturing, an electric arc is employed as the heat source to facilitate layered clad formation. The characteristics of this process, namely the small melt-pool sizes and rapid melting and solidification [17, 18], are well-suited to the material and process properties of Mg-Si alloys. Consequently, the combination of Mg-Si alloys with wire arc additive manufacturing presents a promising avenue for engineering applications.

In this study, the Mg-6wt.% Si (Mg-6Si) specimens were fabricated using wire arc additive manufacturing, employing the gas tungsten arc welding (GTAW) technique with rapid cooling. The morphological characteristics of the intermetallic compound Mg_2Si phase in the Mg-6Si alloy and its impact on the mechanical properties of the alloy were studied. As-cast specimens were also fabricated in a metal mold for comparison. The objective is to refine the Mg_2Si phase within Mg alloys that contain Si, with the aim of offering engineering guidance for the development of high-performance Mg-Si alloys designed for additive manufacturing processes.

2 Experiment

As-cast Mg-6Si alloy specimens for comparison were prepared via metal mold casting with a mixture of 0.5vol.% SF_6 and 99.5vol.% Ar gas in a protected induction furnace. Pure Si was added to the molten Mg at 780 °C, and then, the melt was stirred manually using a steel rod for about 5 min and held for 20 min to dissolve the silicon completely. Finally, the alloy was poured into a steel mold preheated to 250 °C. A rectangular ingot with dimensions of 150 mm×200 mm×120 mm was obtained.

The XJ-500 extruder was used to prepare Φ1.2 mm Mg-6Si alloy as the raw material for the welding wire of GTAW-WAAM, and the substrate was made of magnesium-silicon alloy plate with the size of 100 mm×800 mm×10 mm. In the wire arc additive manufacturing process, an OTC AVP360 frequency AC/DC welder with tungsten argon arc welding was used. Before WAAM, the substrates were ground with sandpapers, degreased with ethanol, and then fixed on a workbench. The welding current used in this study was an alternating current (AC), and the diameter of the tungsten electrode was 2.4 mm.

According to the experimental experiences, the optimized experimental parameters for the additive experiment were a current of 100 A, moving speed of 450 mm·min^{-1}, and interlayer cooling time of 2 min. Argon gas with 99.99% purity and a flow rate of 15 L·min^{-1} was used as the protective gas. The Mg-6Si alloy was deposited on the substrate using a unidirectional scanning strategy. Subsequently, the microstructure, tensile strength, and microhardness of the deposited samples were determined, as shown in Fig. 1.

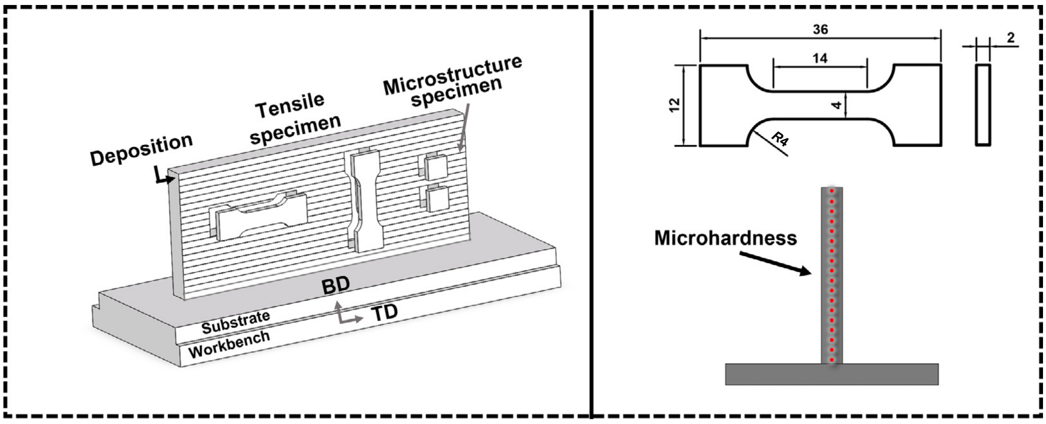

Fig. 1: Schematics of microstructure sample position and tensile specimens (a), dimensions of tensile test samples (unit: mm) (b), and microhardness measurement location (c)

An inductively coupled plasma optical emission spectrometer was used to measure the chemical compositions of the wire and the Mg-6Si WAAM sample, and the results are shown in Table 1. A Vickers hardness tester (HXD-1000TM) was used to measure the Vickers microhardness distribution along the deposition direction at a load of 200 gf with a holding time of 10 s. The spacing between each hardness measurement point was maintained at 500 μm. The tensile mechanical properties were tested at room temperature and 150 °C using a universal testing machine (MTS-CMT5105), with a crosshead speed of 0.1 mm·min^{-1}. Three specimens were tested for each group to obtain reliable results.

Metallographic specimens were cut from the middle region of the deposited layer, and the polished samples were etched with 5% nitric alcohol for 12 s. The metallographic microstructure was examined using an optical microscope (OM), and the microstructure of the deposited layer and fracture surface of the tensile specimens were analyzed using a scanning electron microscope (SEM, JSM-7800F, JEOL) equipped with an energy-dispersive X-ray spectrometer (EDS). The phase constitution of the specimens was confirmed using

Table 1: Chemical compositions of the welding wire and Mg-6Si WAAM sample (wt.%)

Materials	Si	Mg
Wire	5.65	Bal.
WAAM sample	5.92	Bal.

the X-ray diffraction (XRD) analysis. The grain size of the Mg_2Si phase and orientation relationship in the deposited layer were examined via electron backscatter diffraction (EBSD; JSM-7800F, JEOL). The EBSD samples were subjected to Ar-ion polishing with a step size of 0.67 µm.

3 Results

3.1 Mechanical properties

Figure 2(a) presents the tensile properties of the WAAM and as-cast Mg-6Si alloys at room temperature and 150 °C. The average tensile strength of WAAM at room temperature and 150 °C are 140 MPa and 91 MPa, an increase of 63.4% and 21.3%, respectively, over those of the as-cast Mg-6Si sample. The elongation is slightly lower than that of the as-cast state. The alloy exhibits anisotropic tensile properties, with the tensile strength of the longitudinal specimens at room temperature and 150 °C being lower than that of the transversal specimens, as shown in Fig. 2(a). The average microhardness of the WAAM specimen (77.6 HV) is 36.6% higher than that of the cast samples [56.8 HV, Fig. 2(b)].

Figure 3 presents the tensile fracture morphologies of the WAAM Mg-6Si alloy at room temperature and 150 °C. Evidently, the typical brittle fracture features, such as smooth planes with cracks, cleavage planes, and bright white inclusions, indicate that the material is brittle, and the cracks at fracture surface may originate from the interface between the matrix and the inclusions. Smooth planes with cracks are identified as the second phase containing Si, and the bright white inclusions are oxides, as indicated by the EDS mapping results in Fig. 4. In addition, cracks are observed along the boundary of the Si-containing phase, and some of them expand through the interior of this phase. The fracture at room temperature and 150 °C exhibits similar characteristics.

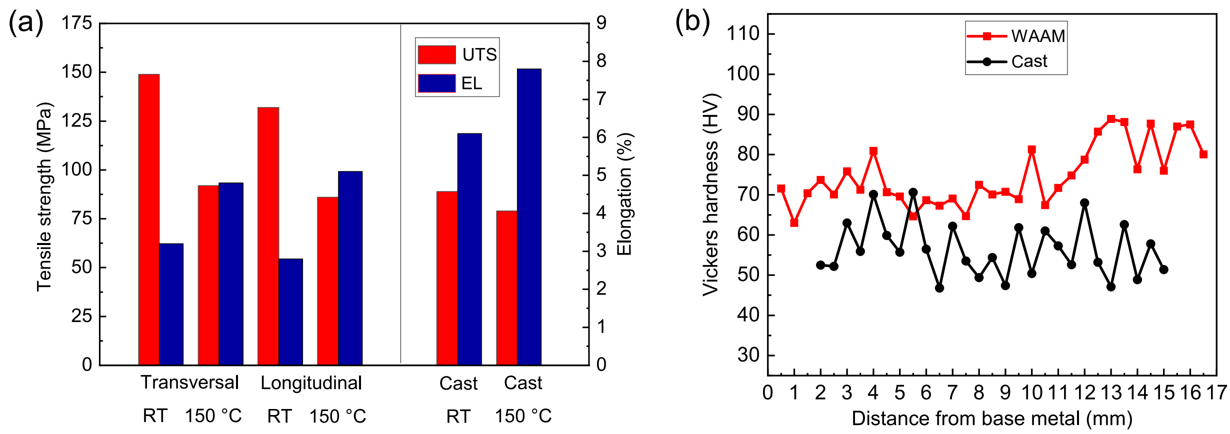

Fig. 2: Mechanical properties (a) of WAAM and as-cast Mg-6Si alloys at room temperature (RT) and 150 °C, and their microhardness distributions (b)

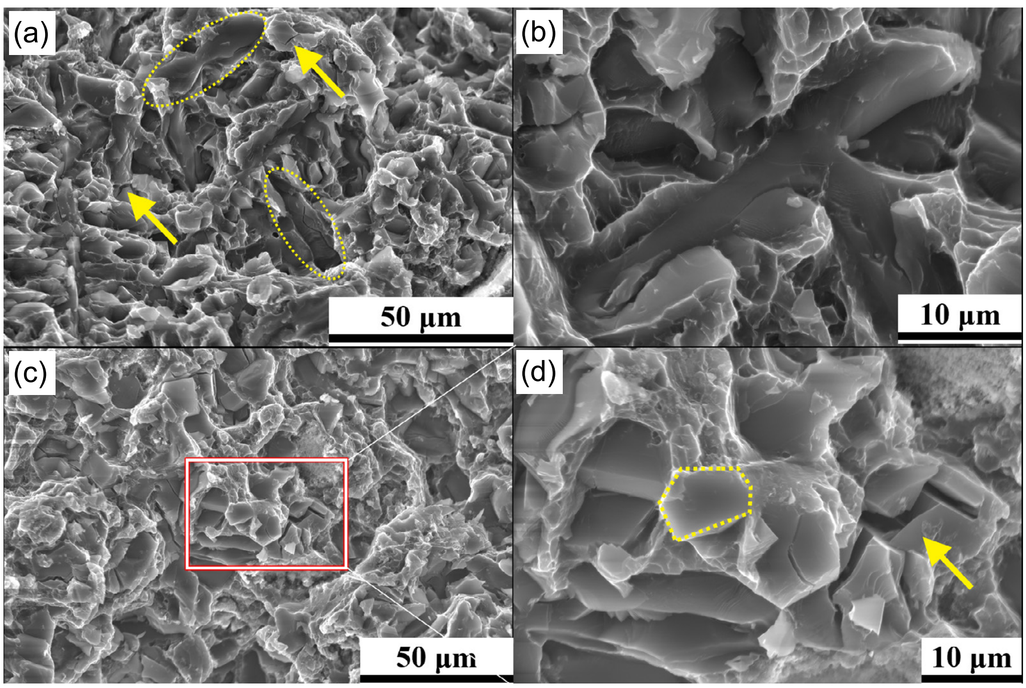

Fig. 3: SEM images showing the fracture morphologies of WAAM tensile samples at room temperature (a, b) and 150 °C (c, d)

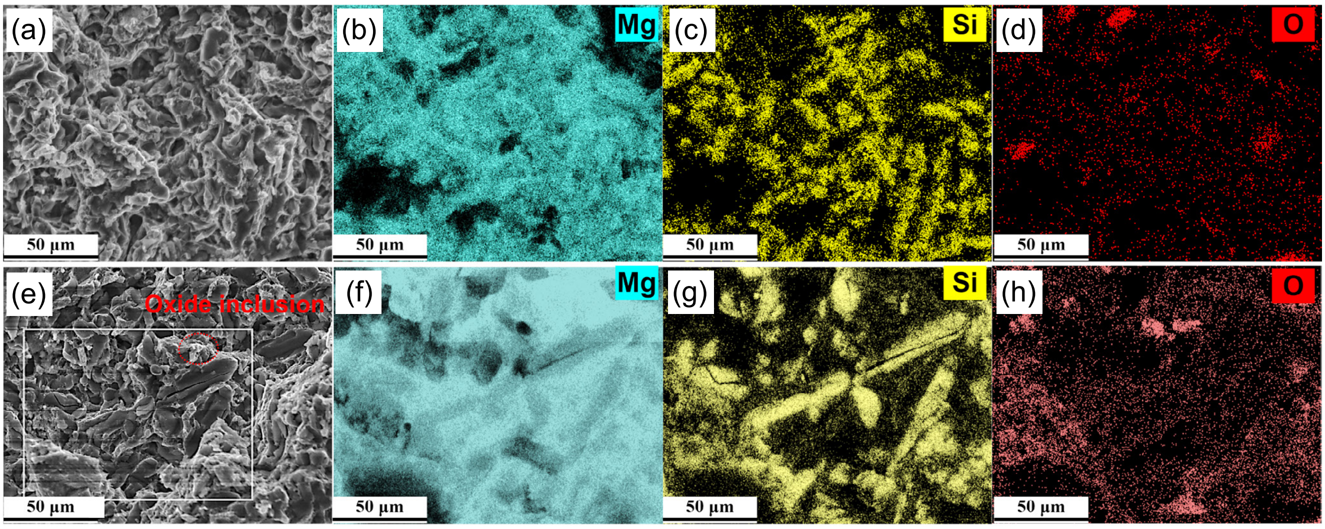

Fig. 4: Fracture morphologies and EDS mapping results of WAAM tensile samples at room temperature (a–d) and 150 °C (e–h)

3.2 Microstructures

Figure 5 presents the XRD analysis results for the as-cast and WAAM Mg-6Si alloys. Evidently, both the as-cast and WAAM Mg-6Si alloys mainly consist of α-Mg and Mg_2Si phases, and no Si peak is observed, indicating that during the preparation process of the specimens, due to sufficient energy and composition fluctuations, sufficient amounts of Si and Mg react to form the secondary phase Mg_2Si. This finding aligns with results reported in a previously reported study [19].

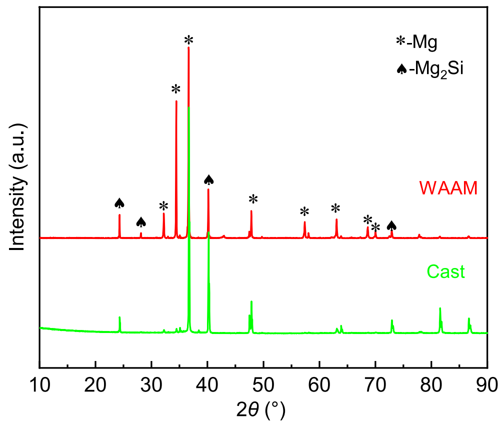

Fig. 5: XRD patterns of as-cast and WAAM Mg-6Si

Figure 6 shows macroscopic optical photographs of the Mg-6Si alloys prepared via wire arc additive manufacturing and conventional casting. No obvious cracks, unfused defects, or other defects are observed on the cross-section of the Mg-6Si alloy in both the as-cast or WAAM state. The secondary phase in the WAAM state mainly consists of numerous equiaxed crystals and some granular phases, whereas in the as-cast state, it mainly consists of massive and granular phases, indicating that there is a significant difference in the kinetic behaviors of phase formation between the two samples in the preparation process. Furthermore, a comparison of the metallographic images of the Mg-6Si alloy in both the as-cast and WAAM samples reveals that metallographs of both the WAAM and as-cast alloys exhibit three different features: black granular particles, gray Chinese-script-type structures with needles, and a bright white matrix.

In this study, two types of Mg_2Si phases are observed: a coarse (intracrystalline) incipient phase precipitated, and a fine (intercrystalline) eutectic phase precipitated subsequently. Based on a previous study [3], XRD and EDS results, and phase diagrams, it is inferred that the black granular particles are the preferential crystalline Mg_2Si phase, the gray Chinese-script-type structures with needles are the eutectic Mg_2Si phase, and the bright white matrix is the α-Mg phase. The black particles in the microstructure of the WAAM samples are finer than those in the as-cast counterparts. Furthermore, the number of diffused black particles in the WAAM samples is larger than those in the as-cast ones. Additionally, their number increases significantly, and the sharp polygonal corners of the boundary are relatively blunt, as shown in Fig. 6(c). Moreover, the gray Chinese-script-type structure with needles that is present in the as-cast state persist after the arc action during welding, but their quantity is significantly reduced, as shown in Figs. 6(d) and (h).

SEM images of the as-cast and WAAM Mg-6Si alloys are presented in Fig. 7. Evidently, the Mg_2Si phase resulting from conventional casting consists of chunky particles and lamellar Chinese-script-type structures, as shown in Figs. 7 and 8. In Fig. 7, the Mg_2Si phase in the WAAM state exhibits regular small granular particles, short rods, dots, and needles precipitated along the inter-dendritic crystals. The EDS results in Table 2 indicate that the regular small particles and fine point- and needle-like particles surrounding them are composed of the Mg_2Si phase. It can also be observed that the Mg_2Si phase is finer and more diffused, which is consistent with the metallographic microstructure observations.

Owing to the large temperature gradient in the melt pool under arc-augmented conditions, the incipient Mg_2Si phase solidifies almost simultaneously, forming an octahedral morphology [9], as shown in Fig. 9. A fraction of α-Mg is separately distributed in and around the incipient Mg_2Si phase, possibly because Mg-6Si is a hypereutectic alloy, and the growth of the Mg_2Si phase in the eutectic microstructure is dependent on the incipient Mg_2Si phase [19]. Moreover, the rapid cooling conditions induced by the electric arc make the solidification behavior of the alloy melt pool deviate from the equilibrium solidification path. This deviation alters the eutectic composition, causing the initially precipitated incipient Mg_2Si phase to solidify rapidly and serve as a heterogeneous nucleation site. Consequently, the α-Mg matrix remains in and around the incipient phase as the temperature decreases during the solidification of the surrounding liquid phase.

Figure 10 shows antipodal plots [inverse pole figure (IPF)] of the EBSD-*YOZ* cross-sections of Mg-6Si alloys in the WAAM and as-cast states, which are derived from a statistical analysis of the grain size distribution. The maximum grain size of the as-cast specimen is greater than 165 μm, whereas that of the WAAM specimen is smaller than 95 μm. The average grain size of the Mg-6Si specimens in the as-cast state is 51.36 μm, which is 3.5 times larger than that of the WAAM specimen, with an average grain size of 14.77 μm.

The maximum size of the as-cast Mg_2Si phase is 127 μm, whereas that of the WAAM Mg_2Si phase does not exceed 45 μm. The average sizes of the Mg_2Si phase in as-cast and WAAM specimens are 42.88 μm and 9.20 μm, respectively. The average size of WAAW alloy is decreased by nearly 5 times compared to that of as-cast alloy.

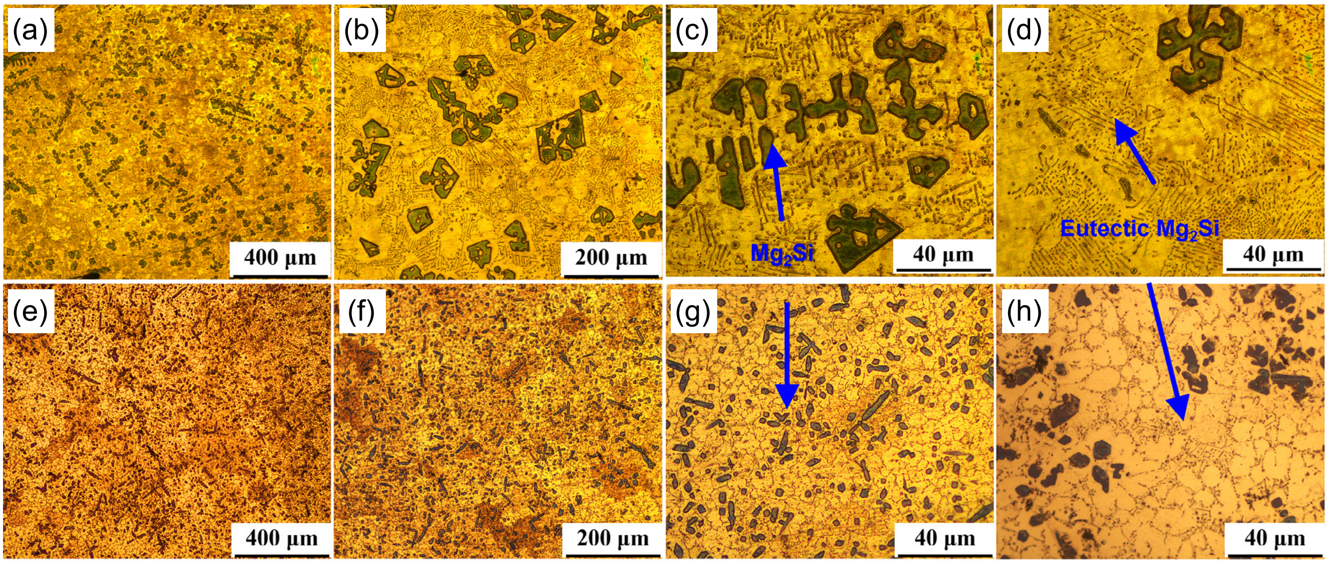

Fig. 6: OM images of as-cast (a–d) and WAAM (e–h) Mg-6Si alloys

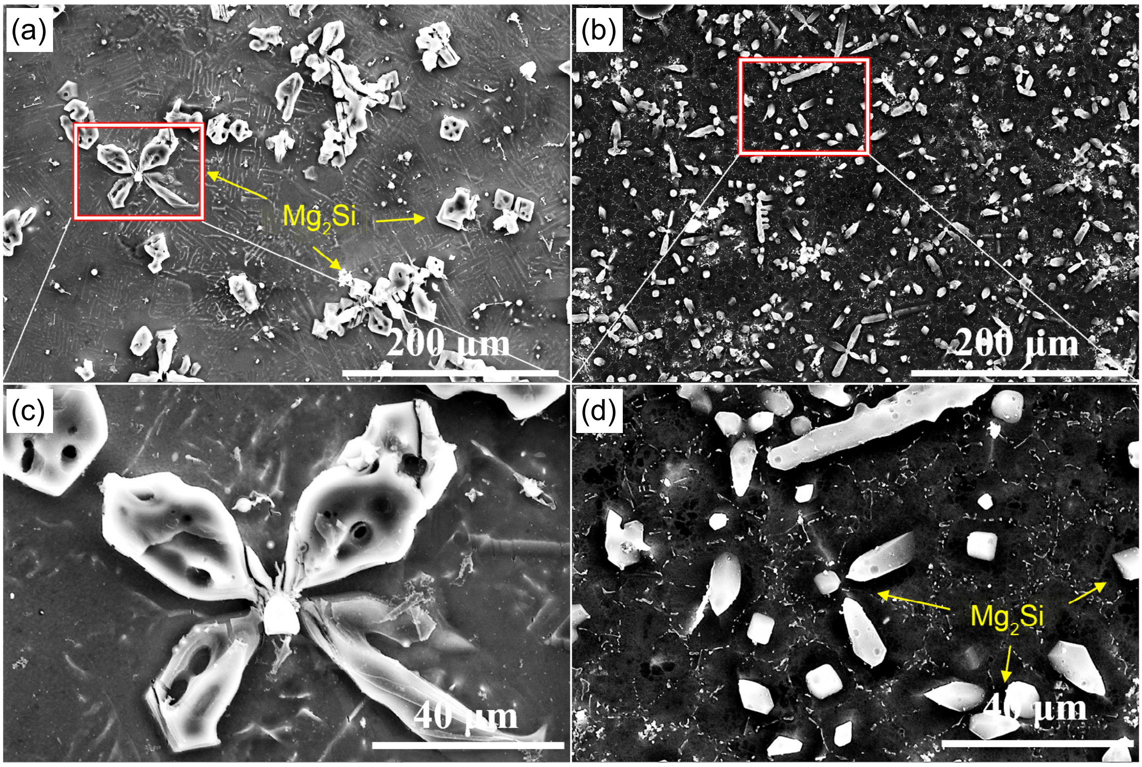

Fig. 7: Microstructures of as-cast (a, c) and WAAM (b, d) Mg-6Si alloys

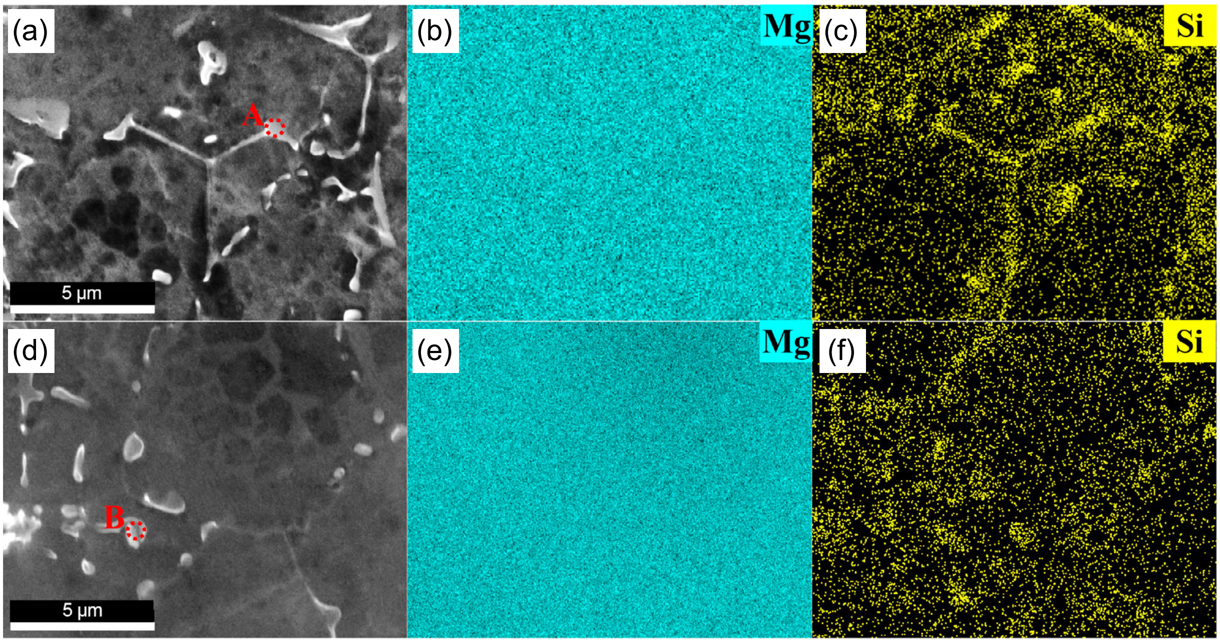

Fig. 8: SEM images of the eutectic Mg_2Si phase in as-cast (a–c) and WAAM (d–f) alloys

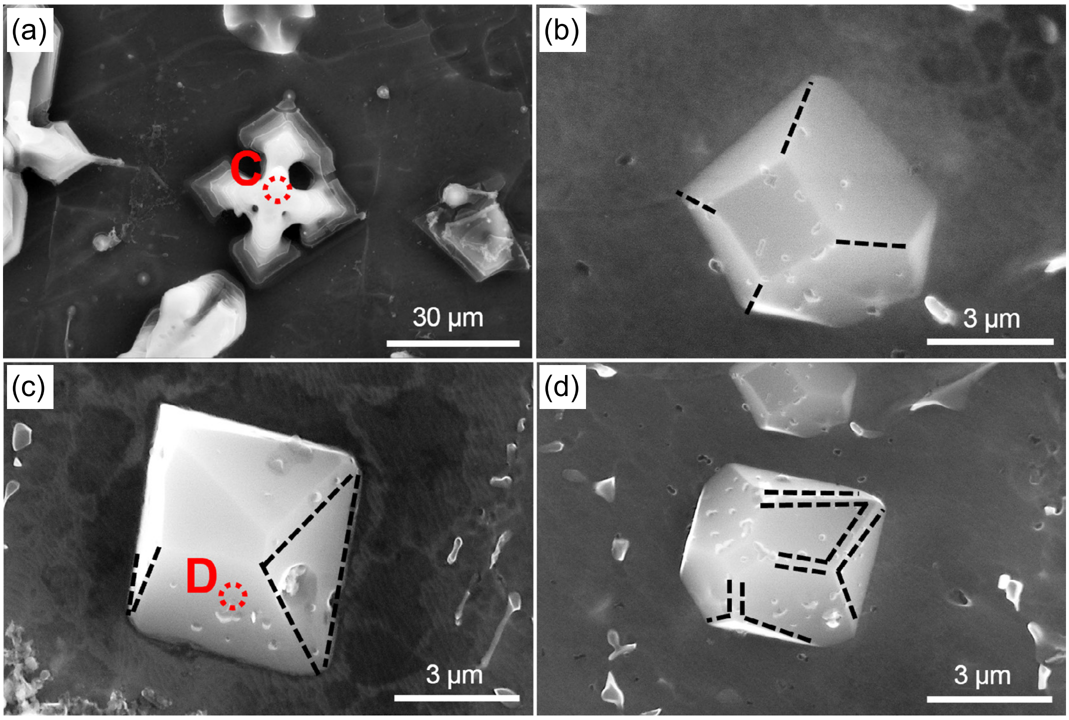

Fig. 9: SEM images of the primary Mg_2Si phase in as-cast (a, c) and WAAM (b, d) alloys

Table 2: EDS analyses of Positions A, B, C, and D indicated in Figs. 8 and 9

Position	Chemical composition (at.%)	
	Mg	Si
A	97.65	2.35
B	94.57	5.43
C	66.30	33.70
D	67.51	32.49

4 Discussion

4.1 Strengthening and fracture of WAAM Mg-6Si alloys

The morphology and size of the secondary phase affect mechanical properties of the alloys. The beneficial impact of the finely dispersed secondary phases on the mechanical properties of the material is evident. The high-temperature arc generated by the arc additive welding causes rapid cooling, resulting in dissolution of the Mg_2Si phase, and consequently, Si and Mg are redistributed in the alloy owing to diffusion. The

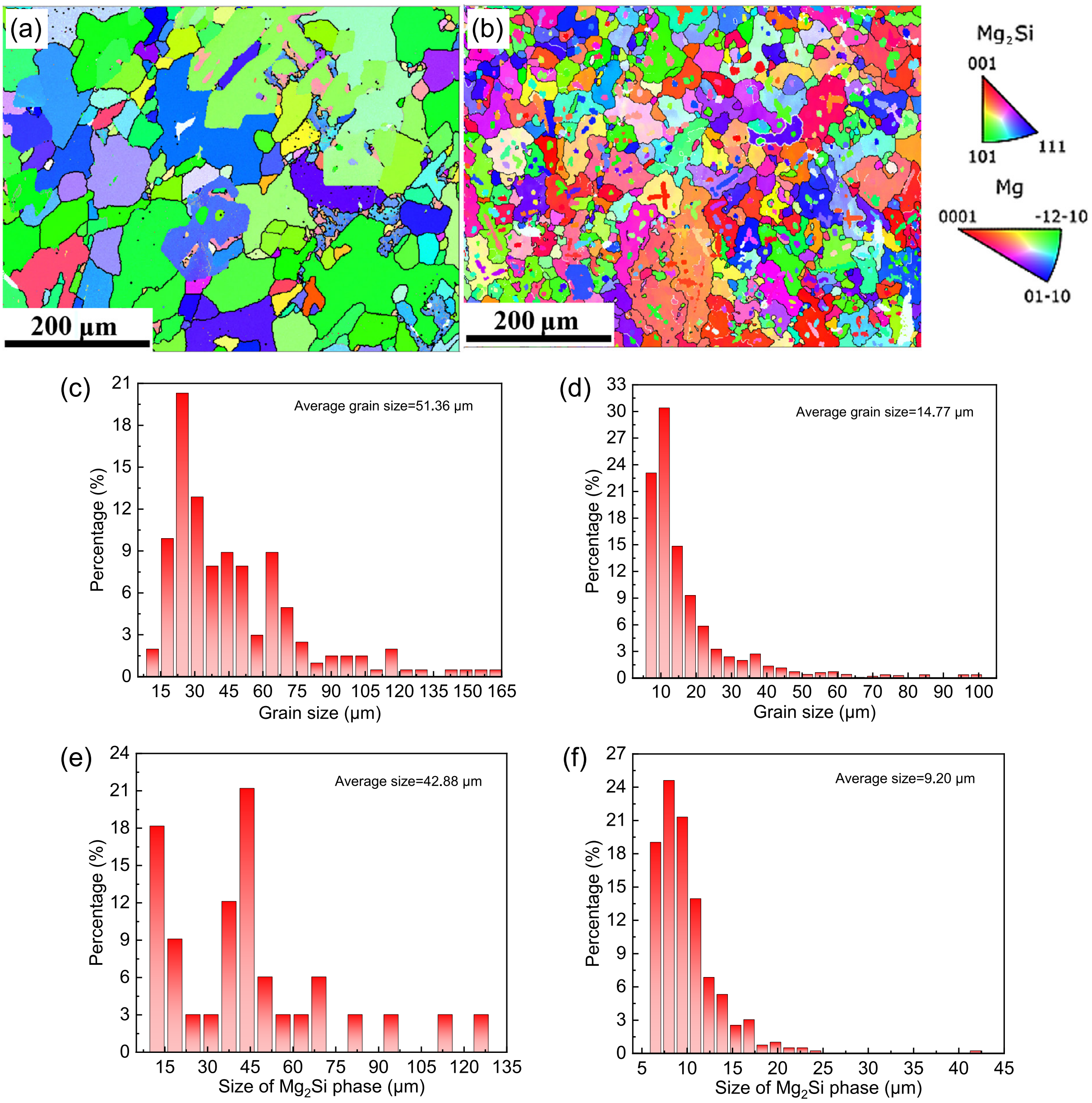

Fig. 10: EBSD IPF maps and statistics of the grain size of as-cast (a, c, e) and WAAM (b, d, f) Mg-6Si alloys

size and morphology of the Mg_2Si crystals undergo changes from their initial as-cast state, attributed to the in situ formation of Mg_2Si crystals during the rapid cooling process. The grain refinement is the result of two processes: grain nucleation and grain growth. After rapid cooling, the incipient Mg_2Si phase is formed preferentially over the α-Mg phase owing to its higher melting point. According to the metal solidification theory [20]:

$$\frac{G}{v} < \frac{mC_0}{D}\frac{1-k}{k} \quad (1)$$

where G represents the thermal temperature gradient, v represents the solidification rate, m is the slope of the liquids phase line, D is the diffusion coefficient, C_0 represents the solute concentration, and k is the equilibrium partition coefficient. Increased supercooling reduces the critical nucleation radius and nucleation work, leading to the formation of numerous nuclei. Additionally, rapid solidification and short-term growth conditions restrict the kinetic behavior of grains, resulting in refinement. Furthermore, under external stresses, the smoothing of sharp corners reduces the degree of penetration of grain boundaries into the matrix and slows the expansion of cracks, thereby improving the mechanical properties. Moreover, the increase in the specific surface area of the finely dispersed incipient Mg_2Si phase leads to an enhancement in plugging due to the presence of dislocation movements during the deformation of the material under the application of external force. This results in an increased bonding strength at the interface between Mg_2Si and Mg. According to the classical Hall-Petch relationship, there is a synergistic effect of refinement strengthening and dispersion strengthening throughout the microstructure. Notably, the observed superior strength and hardness of the Mg-6Si alloy in the WAAM state, compared to those in the as-cast state, can be attributed to this synergistic effect. The results of the present study indicate that WAAM is effective for grain refinement and strengthening of Mg alloys.

In addition, there is a substantial reduction in the amount of acicular Mg_2Si phases in the WAAM samples compared with their as-cast counterparts, which enhances the mechanical properties of the alloy, as shown in Fig. 5. The coarse acicular Mg_2Si phase tends to function as a crack initiation point in the alloy, when subjected to external forces, the acicular structure tends to cause stress concentration. Thus, cracks initiate and propagate along the acicular phase, leading to the premature failure of the Mg-6Si alloy before it achieves its anticipated properties.

Figure 11 shows the EBSD kernel average misorientation (KAM) plots and their distributions for as-cast and WAAM Mg-6Si alloys. The KAM plot shows the distribution of the mean orientation difference, with blue color indicating a small KAM value and red color indicating a large KAM value, suggesting a higher defect density or residual stress. As shown in Fig. 11(b), there are more green distributions at the interface between the Mg_2Si phase and the α-Mg matrix, indicating a high dislocation density and significant stress concentration between the Mg_2Si phase and the α-Mg matrix [21, 22], which suggests that the subsequent cyclic repetitive heating does not completely eliminate the internal stresses of the wire arc additive manufacturing process. Under external stresses, small cracks typically form at the interfaces between phases where the stresses are concentrated. These cracks then propagate through both the Mg_2Si phase and the α-Mg interface, resulting in material failure. In addition to the tensile fracture shown in Fig. 3, the cracks expand along the phase interface, exhibiting characteristics of intergranular fracture. Furthermore, some of them pass through the coarse incipient Mg_2Si phase when expanding, exhibiting characteristics of transgranular fracture, as indicated by the yellow arrows in Fig. 4.

The mechanical properties of the Mg-6Si alloys processed using wire arc additive manufacturing in the present study are still not satisfactory. However, there is a significant improvement compared to the as-cast state, with the average tensile strengths of the WAAM Mg-6Si alloy increasing by 63.4% at room temperature and by 21.3% at 150 °C. Additionally, the hardness is increased by 36.6% when compared to the as-cast state. Future enhancements in the mechanical properties of Mg-Si alloys can be achieved by refining the Mg_2Si phase under arc conditions to reduce internal stresses.

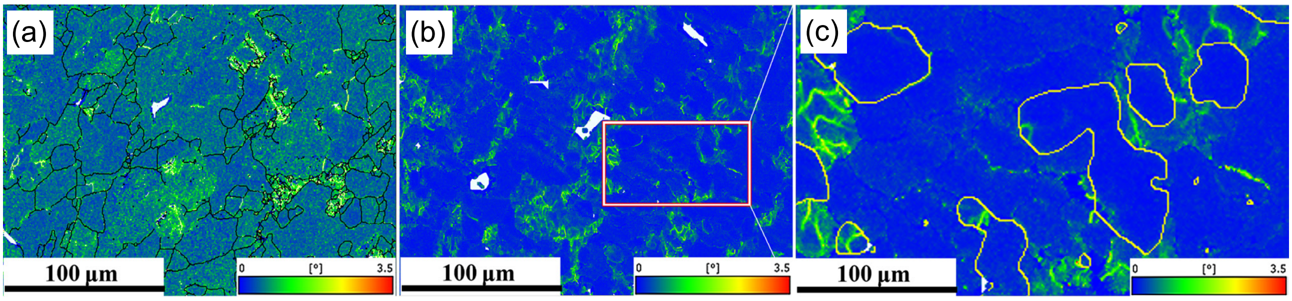

Fig. 11: EBSD KAM diagram and distribution of Mg-6Si in the as-cast (a) and WAAM (b, c) states

4.2 Orientation relationship between Mg_2Si phase and α-Mg matrix phase

The orientation distribution information of the Mg_2Si phase and the α-Mg matrix phase was obtained by EBSD (Fig. 12). A total of 50 crystal distributions of the Mg_2Si phase and the surrounding α-Mg matrix were counted to ensure the accuracy of the results. Analysis using Aztec software identified no clear orientation relationship between Mg_2Si and α-Mg under the action of arc.

Furthermore, this study presents several orientation relationships between the Mg_2Si phase and α-Mg, with reference to earlier studies on orientation relationships in Mg-Si systems. For instance, Yang et al. [23] identified a specific orientation relationship between Mg_2Si and the α-Mg matrix in the Mg-5Sn-2Si-1.5Al-1Zn-0.8Sb alloy through TEM, e.g., (220) Mg_2Si || $(0\bar{1}12)$ α-Mg, [001] Mg_2Si || $[01\bar{1}1]$ α-Mg. Fritz et al. [24] observed the following orientation relationships: (0001) α-Mg || (010) Mg_2Si, $[01\bar{1}0]$ α-Mg || [001] Mg_2Si. Ding et al. [25] employed friction stir processing (FSP) to prepare Mg-Al composite plates and found that the orientation relations of Mg_2Si and α-Mg were $(\bar{1}100)$ α-Mg || $(\bar{2}\bar{1}0)$ Mg_2Si, $[22\bar{4}1]$ α-Mg || [001] Mg_2Si. The orientation relationships of

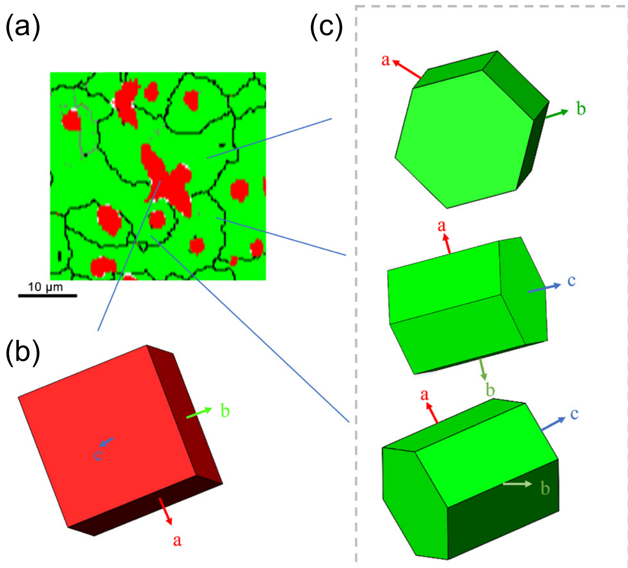

Fig. 12: EBSD analysis of the crystallographic orientation of the Mg_2Si phase and surrounding α-Mg matrix in wire arc additive manufacturing (a), including the orientations of the Mg_2Si phase (b), and the surrounding α-Mg matrix (c)

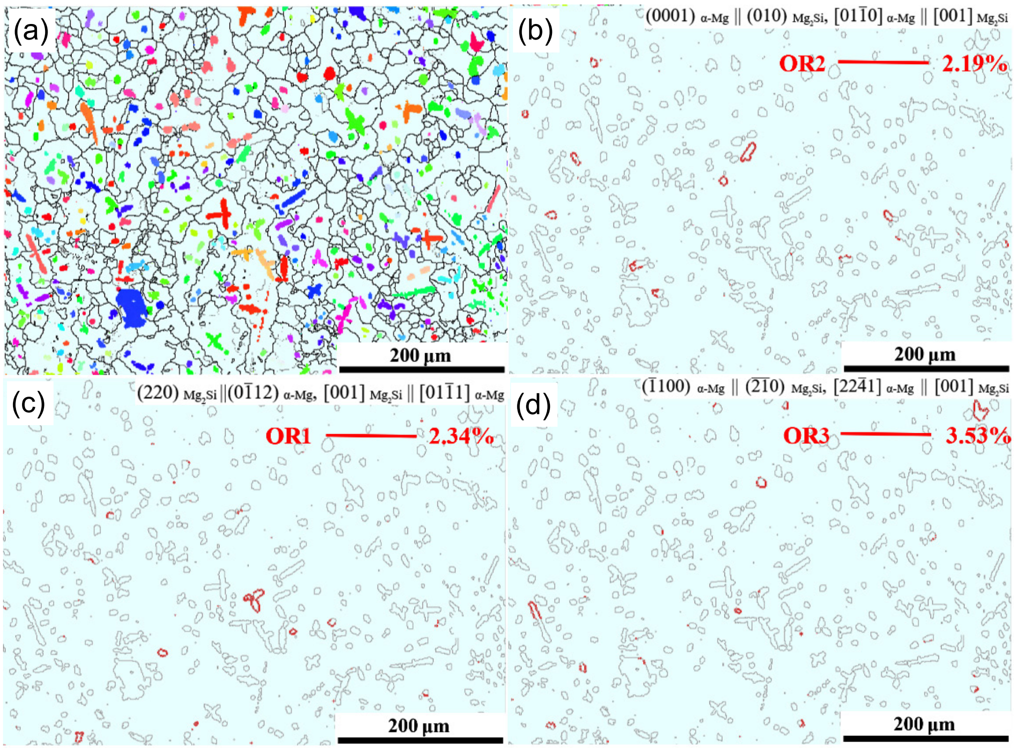

Fig. 13: EBSD distribution of the Mg_2Si phase of the WAAM alloy with inverse pole figure (IPF) color (a), and statistical plots of the proportion of special crystallographic orientations (b), (c), and (d)

Mg_2Si phase and α-Mg known in the above three studies were denoted respectively as OR1, OR2, and OR3, respectively.

These orientation relationships were analyzed using Aztec (Fig. 13). Figure 13(a) shows the EBSD distribution of the Mg_2Si phase in the WAAM state with antipodal map color distribution; Figs. 13(b), (c), and (d) show statistical plots of the proportions with different specific crystallographic orientations.

The proportions of OR1, OR2, and OR3 in the Mg-6Si prepared by wire arc additive manufacturing are 2.34%, 2.19%, and 3.53%, respectively. Statistically, it can be assumed that the Mg-6Si samples prepared by wire arc additive manufacturing do not have a specific crystallographic orientation relationship.

5 Conclusions

(1) The microstructure of Mg-6Si alloys fabricated via wire arc additive manufacturing consists of acicular and granular Mg_2Si phases and α-Mg. In contrast, the Mg_2Si phase formed under conventional casting consists of coarse massive lamellar Chinese-script-like phases.

(2) The average tensile strengths of WAAM specimens at room temperature and 150 °C are 140 MPa and 91 MPa, an increase of 63.4% and 21.3%, respectively, over those of the as-cast Mg-6Si. However, the elongation is slightly lower than that of the as-cast state. The alloy exhibits anisotropic tensile properties, with the tensile strength of the longitudinal specimens at room temperature and 150 °C being lower than that of the transversal specimens. The WAAM specimens present an average microhardness of 77.6 HV, 36.6% higher than that of the as-cast specimens (56.8 HV).

(3) There are significant stresses at the interface between the Mg_2Si phase and α-Mg, and the cracks at the tensile fracture expand along this interface. Some cracks pass through the coarse Mg_2Si phase during expansion, exhibiting a mixture of transgranular and intergranular fractures.

(4) WAAM refines both the Mg_2Si phase and the overall grain resulting in a more homogeneous morphology and improved mechanical properties. No discernible orientation relationship is observed between Mg_2Si and α-Mg. In the WAAM state, the acicular Mg_2Si phase is distributed along the grain boundaries, and present in a significantly reduced quantity compared to the as-cast state. In contrast, the granular Mg_2Si phase is finer and more dispersed, with a considerably higher amount. The average grain size of the Mg_2Si phase is about 9.20 μm, which is about 5 times smaller than that of the as-cast alloy.

Acknowledgments

This research was supported by the National Natural Science Foundation of China (Grant Nos. 52001037, U2037601, and U21A2048) and the Science and Technology Program of Guangzhou, China (Grant No. 2022BLC003). The authors also would like to thank Roshen for providing language help.

Conflict of interest

Prof. Bin Jiang is an EBM of *CHINA FOUNDRY*. He was not involved in the peer-review or handling of the manuscript. The authors have no other competing interests to disclose.

References

[1] Yang Y, Xiong X, Chen J, et al. Research advances in magnesium and magnesium alloys worldwide in 2020. Journal of Magnesium and Alloys, 2021, 9(3): 705–747. https://doi.org/10.1016/j.jma.2021.04.001

[2] Pollock T M. Weight loss with magnesium alloys. Science, 2010, 328(5981): 986–987. https://doi.org/10.1126/science.1182848

[3] Jamalpour M, Alizadeh R. Effects of heat treatment and Y addition on the microstructure and mechanical properties of as-cast Mg-Si alloys. Materials Science and Engineering: A, 2022, 859: 144209. https://doi.org/10.1016/j.msea.2022.144209

[4] Alizadeh R, Mahmudi R. Effects of Sb addition on the modification of Mg_2Si particles and high-temperature mechanical properties of cast Mg-4Zn-2Si alloy. Journal of Alloys and Compounds, 2011, 509(37): 9195–9199. https://doi.org/10.1016/j.jallcom.2011.06.109

[5] Cui B, Yang L, Deng Y L, et al. Effect of adding elements on microstructure of Mg-3Si alloy. Jouranl of Materials Engineering, 2017, 45(3): 95–101. https://doi.org/10.11868/j.issn.1001-4381.2015.000136. (In Chinese)

[6] Jiang Q C, Wang H Y, Wang Y, et al. Modification of Mg_2Si in Mg-Si alloys with yttrium. Materials Science and Engineering: A, 2005, 392(1–2): 130–135. https://doi.org/10.1016/j.msea.2004.09.007

[7] Zhang E, Wei X, Yang L, et al. Effect of Zn on the microstructure and mechanical properties of Mg-Si alloy. Materials Science and Engineering: A, 2010, 527(13–14): 3195–3199. https://doi.org/10.1016/j.msea.2010.01.074

[8] Tang S Q, Zhou J X, Tian C W, et al. Morphology modification of Mg_2Si by Sr addition in Mg-4% Si alloy. Transactions of Nonferrous Metals Society of China, 2011, 21(9): 1932–1936. https://doi.org/10.1016/S1003-6326(11)60952-7

[9] Chen L, Wang H Y, Li Y J, et al. Morphology and size control of octahedral and cubic primary Mg_2Si in an Mg-Si system by regulating Sr contents. CrystEngComm, 2014, 16(3): 448–454. https://doi.org/10.1039/C3CE41646A

[10] Hou J, Li C, Liu X. Nucleating role of an effective in situ Mg_3P_2 on Mg_2Si in Mg-Al-Si alloys. Journal of Alloys and Compounds, 2011, 509(3): 735–739. https://doi.org/10.1016/j.jallcom.2010.09.039

[11] Yang W, Wang Y, Cui H, et al. Primary Mg_2Si phase and Mg_2Si/α-Mg interface modified by Sn and Sb elements in a Mg-5Sn-2Si-1.5 Al-1Zn-0.8Sb alloy. Journal of Magnesium and Alloys, 2022, 10(11): 3234–3249. https://doi.org/10.1016/j.jma.2021.02.003

[12] Mirshahi F, Meratian M, Panjepour M. Microstructural and mechanical behavior of Mg/Mg_2Si composite fabricated by a directional solidification system. Materials Science and Engineering: A, 2011, 528(29–30): 8319–8323. https://doi.org/10.1016/j.msea.2011.07.057

[13] Yang R, Chen K, Wen S, et al. Enhanced strength and hardness of AS41 magnesium alloy fabricated by selective laser melting. Materials, 2022, 15(17): 5863. https://doi.org/10.3390/ma15175863

[14] Kang J, Wang K, Jing X R, et al. Research progress of Mg_2Si phase regulation in magnesium-based materials. Materials Reports, 2022, 36(22): 22030308-7. https://doi.org/10.11896/cldb.22030308

[15] Saleh B, Fathi R, Tian Y, et al. Fundamentals and advances of wire arc additive manufacturing: Materials, process parameters, potential applications, and future trends. Archives of Civil and Mechanical Engineering, 2023, 23(2): 96. https://doi.org/10.1007/s43452-023-00633-7

[16] Li Q Z, Zhang H Z, Wang S, et al. Research progress in additive manufacturing technology of magnesium alloys. Journal of Materials Engineering, 2023, 51(11): 34–51. https://doi.org/10.11868/j.issn.1001-4381.2021.001133. (In Chinese)

[17] Wang Z, Wang J, Lin X, et al. Solidification microstructure evolution and its correlations with mechanical properties and damping capacities of Mg-Al-based alloy fabricated using wire and arc additive manufacturing. Journal of Materials Science & Technology, 2023, 144: 28–44. https://doi.org/10.1016/j.jmst.2022.10.019

[18] Tong X, Wu G, Easton M A, et al. Microstructural evolution and strengthening mechanism of Mg-Y-RE-Zr alloy fabricated by quasi-directed energy deposition. Additive Manufacturing, 2023, 67: 103487. https://doi.org/10.1016/j.addma.2023.103487

[19] Tanhaee Z, Mahmudi R. The microstructure and creep characteristics of cast Mg-3Si and Mg-3Si-1Gd alloys. Materials Science and Engineering: A, 2016, 673: 148–157. https://doi.org/10.1016/j.msea.2016.07.026

[20] Fan G, Su H, Zhang J, et al. Microstructure and cytotoxicity of Al_2O_3-ZrO_2 eutectic bioceramics with high mechanical properties prepared by laser floating zone melting. Ceramics International, 2018, 44(15): 17978–17985. https://doi.org/10.1016/j.ceramint.2018.06.275

[21] Lee J, Terner M, Copin E, et al. A novel approach to the production of NiCrAlY bond coat onto IN625 superalloy by selective laser melting. Additive Manufacturing, 2020, 31: 100998. https://doi.org/10.1016/j.addma.2019.100998

[22] Cheng S, Liu F, Xu Y, et al. Effects of arc oscillation on microstructure and mechanical properties of AZ31 magnesium alloy prepared by CMT wire-arc directed energy deposition. Materials Science and Engineering: A, 2023, 864: 144539. https://doi.org/10.1016/j.msea.2022.144539

[23] Yang W, Wang Y, Cui H, et al. Primary Mg_2Si phase and Mg_2Si /-Mg interface modified by Sn and Sb elements in a Mg-5Sn-2Si-1.5Al-1Zn-0.8Sb alloy. Journal of Magnesium and Alloys, 2022, 10(11): 3243–3249. https://doi.org/10.1016/j.jma.2021.02.003

[24] Grensing F C, Fraser H L. Structure and properties of rapidly solidified magnesium-silicon alloys. Materials Science and Engineering, 1988, 98: 313–319. https://doi.org/10.1016/0025-5416(88)90177-2

[25] Ding Z, Li Z, Li H, et al. Microstructure of Mg solid solution layer during multi-pass FSP of Mg/Al composite plates. Vacuum, 2020, 172: 109078. https://doi.org/10.1016/j.vacuum.2019.109078